

# Structural and Energetic Stability of the Lowest Equilibrium Structures of Water Clusters

Vishwa K. Bhatt,\* Sajeev S. Chacko, Nitinkumar M. Bijewar, and Balasaheb J. Nagare†

*Department of Physics (Autonomous), University of Mumbai,  
Kalina Campus, Santacruz (East), Mumbai-400 098, India.*

(Dated: November 4, 2024)

In the present work, the low-lying structures of 20 different sized water clusters are extensively searched using the artificial bee colony algorithm with TIP4P classical force field. To obtain the lowest equilibrium geometries, we select the 10 lowest configurations for further minimization using density functional theory. The resulting structures are lower in energy than previously reported results. The structural and energetic stability of these clusters are studied using various descriptors such as binding energy, ionization potentials, fragmentation energy, first and second energy difference, vibrational and optical spectra. The energetic analysis shows that clusters with  $N = 4, 8, 12, 14, 16$  and  $19$  are more stable. The analysis of fragmentation energies also supports these findings. Our calculations show that non covalent interactions play a significant role in stabilizing the water clusters. The infrared spectra of water clusters display three distinct bands: intermolecular O...H vibrations ( $23\text{--}1191\text{ cm}^{-1}$ ), intramolecular H-O-H bending ( $1600\text{--}1741\text{ cm}^{-1}$ ) and O-H stretching ( $3229\text{--}3877\text{ cm}^{-1}$ ). The strongest intensity is observed in the low-frequency symmetric stretching modes, along with a noticeable red-shift in the stretching vibrations. The optical band gap ranges from  $7.14\text{ eV}$  to  $8.17\text{ eV}$  and lies in the ultraviolet region. The absorption spectra also show line broadening for clusters with  $n \geq 10$ , resulting in an increase in spectral lines. Interestingly, only the stable clusters exhibit maximum oscillator strength, with the first excitation in all cases corresponding to a  $\pi \rightarrow \sigma^*$  transition.

## I. INTRODUCTION

Every aspect of our daily lives is influenced by water due to its various unique properties and characteristics, suitable for the origin of life and its abundance in nature. It has been of prime importance due to its broad range of physicochemical properties paving the way towards various technological processes [1] such as corrosion, lubrication, heterogeneous catalysis and electrochemistry. It further helps to understand how different biological and geological processes are carried out, its major role in the operation of hydrogen fuel cells, as well as in advancing technological development at the nanoscale [2].

Water clusters are found everywhere in nature, in the form of clouds, atmosphere, oceans etc [3]. These are formed due to various reasons like the presence of dust particles in the atmosphere, various micro- and nano-sized impurities, bio-waste, and solutes in the seawater. Depending upon these factors and various other factors like temperature, pressure etc around them, and the dimensions and the chemical properties of the surface or volume surrounding them, different-sized water clusters are formed, e.g. dimers, trimers etc. to clusters with  $n$ -molecules. These clusters with  $n$ -number of molecules have different bond lengths and bond angles, which lead to different physical and chemical processes observed in nature. It is found that the absorption of UV radiation in the atmosphere has led to many phenomena like

water splitting, making available hydrogen and oxygen,  $\text{OH}^-$ ,  $\text{H}^+$  and other species [3]. Recently, it has been observed that the smallest size of water cluster [4] in which ice can form, is of 90 water molecules, where they have also studied the characteristic hydrogen bonding of ice-I between 90 water molecules using theoretical methods and experimental infrared spectroscopy, and found that in the range of clusters between 90 to 150 molecules, at a little below freezing temperature, there is a coexistence of crystalline and amorphous clusters and they exhibit hetero-phasic oscillations in time [5]. It has also been seen that in biological systems, water molecules form an unlimited hydrogen-bonded network with structured clustering [6] and influences chain folding [7], internal dynamics, conformational stability, binding specificity and catalysis [8].

It has been observed that despite its simple molecular structure, water clusters provide a challenging problem to study since they involve a rather complicated interplay of various interactions, including vibration, bending and electrostatic interactions as well as Lennard-Jones (LJ) type interactions and complicated potential energy surfaces [9]. The study of the finite-size water clusters provides more accurate models of water, which may lead to an improved understanding of bulk water. Water clusters can be considered as a bridge between the gas and the condensed phases, and therefore, the evolution towards condensed phase structure and their dynamics as a function of size is of interest [10]. A past study shows that the water clusters have played an important role in atmospheric and space chemistry [11], and therefore, cluster studies may contribute to the understanding of the pertinent processes.

\* vishwa\_bhatt@yahoo.com

† corresponding author; bjnagare@gmail.com

There have been numerous experimental and theoretical works on various properties and characteristics of water systems. It is the most studied system compared to any other. Debenedetti *et al.* have studied the polyamorphism of water and observed supercooled and glassy states well below the freezing point of ice which have been a much-debated topic for the last 30 years [12, 13]. A recent study [14] on unconventional nano-rheology and the high viscosity of melt-water shows two orders of magnitude greater than water in pristine form, leading to slippery ice which is another unique feature of water. To understand these unique phenomena, one needs to go down to the molecular level and study the intermolecular interactions, orientations of atoms, coordination, bonding etc.

Over the years, studies have been performed at classical scale as well as using *ab initio* methods. Geometry optimizations of water clusters have been performed by various methods including density functional theory (DFT) with the Becke’s three-parameter exchange functional along with the Lee-Yang-Parr correlation functional (B3LYP) [15], second-order Møller-Plesset perturbation theory (MP2), complete active space self-consistent field (CASSCF), coupled cluster singles and doubles (CCSD) approaches and multiconfigurational complete active space second-order perturbation theory (CASPT2). It has been found [16] that CCSD gave the best result of 0.01 Å of the average deviation of O-O distances in the water clusters studied as compared to the Hartree-Fock (HF) and CASSCF, which do not involve dynamic electron correlation. In the past, researchers have used a combination of various methods to improve the accuracy of the results. For example, geometry optimization was performed using the MP2 method and the energy calculation was done by 6-311++G(d,p) [17], the vertical ionization potential (VIP) and the adiabatic ionization potential (AIP) have been studied using BHandHLYP/6-31++G\*\*, double hybrid B2GP-PLYP and CCSD(T) [16] method, whereas the calculation of ionization potential and excitation were done with the help of B3LYP/cc-pVTZ, standard equation of motion coupled cluster singles and doubles (EOM-CCSD) and time-dependent density functional theory (TDDFT) [18].

Despite the vast literature available on water clusters in the past, there has always been an interest among researchers in order to keep improving their methods to find the best model for water clusters [19–25] such that their calculated values are close to the experimentally obtained results. It is mentioned in the literature that the HCTH functionals [26] turn out to be better than BLYP mainly because of the greater number of parameters that refine the correlation part. The HCTH functional is known to give extremely accurate results for the structures and energies for various systems tested. It

was specifically developed to improve its performance for weak interactions. It contains 15 parameters, which are refined over a training set of 407 molecules, which includes H<sub>2</sub>O, (H<sub>2</sub>O)<sub>2</sub>, and H<sub>2</sub>O<sup>+</sup> molecules. The comparison between the hybrid, meta-GGA and GGA functionals like B97-1, B3LYP, B98, VSXC and HCTH/407, also indicated lowest RMS errors for HCTH/407 with respect to the energies of the anionic and cationic systems, as well as for the ionization potentials and electron affinities. The sum of gradient errors, the shift of the H-bond lengths for H-bonded dimers also show low RMS errors [27–30].

Thus, as the HCTH functional shows promising results, we have used this functional to test its validity, where we confirmed the structural and electronic properties of water clusters. We found the bond length, bond angles values for monomer and dimeric systems were close to those measured experimentally [31–34]. For example, for monomer, we obtained, O-H=0.957 Å and H-O-H=104.586° whereas the experimental values in the literature are O-H=0.957 Å and H-O-H=104.5°. Also, our values are better than the other theoretical values as listed in the references [31] and [32]. In the case of dimer, we obtained d(O-O)=3.01 Å which is close to the experimental value of 2.976 Å and with the theoretical values reported [31]. The binding energy for dimer that we obtained is -5.307 kcal/mol which is close to the experimental value of -5.4±0.7 kcal/mol [33]. Also, the experimental ionization potential for a water monomer reported in literature is 12.6 eV [34], whereas the value we got is 12.85 eV.

We have also performed an extensive search for global minima of water clusters, for number of molecules with  $n = 1 - 20$ , employing *ab initio* density functional theory (DFT). We report the minimum energy structures as compared to many extensive works [35–39]. In addition, we further extend our study to present various other findings of these global minima, which includes structural properties, energetics, bonding, ionization potentials, fragmentation patterns and an interplay between them. We have also presented their optical and vibrational properties, and hence presented a comprehensive study to understand the trend exhibited by water clusters as they evolve in size, from  $n = 1$  to 20.

The organization of the present paper is as follows. In section II, we will describe the model and technical details of our simulations. In section III, we present and discuss the results. In section IV, we will summarize our results along with some important concluding remarks.

## II. METHODOLOGY

We have carried out series of calculations on water clusters with  $n = 1 - 20$ . To begin with, we have obtained low energy isomers using artificial bee colony algorithm of ABCluster package [40] with TIP4P force field potential [41]. After eliminating the structures with similar energies ( $\Delta E < 0.01$  eV) from tens of thousands of structures, we found at least 200 distinct structures. Out of these a minimum of 10 lowest energy structures were further optimized using the Gaussian 03 package [42] with the HCTH/407 functional and the 6-311++G(d,p) basis set [43].

The optimized coordinates for  $(\text{H}_2\text{O})_n$  clusters, for  $n = 1 - 20$  from the Cambridge Cluster Database (CCD) [44] were compared with those obtained by our calculations. The stacked pentagonal and cage-like structures were found to be lower in energies for  $n = 11, 13 - 20$  as against the stacked cubic structures available in the CCD. For  $n = 1 - 20$ , many different conformers were considered out of which the ones we have reported in Figure 1 turn out to be the lowest energy structures. The coordinates of the lowest energy structures are given in the supplementary material.

We report here that with the level of exchange correlation used in the present work gives lowest energies as compared with the recent extensive global minima reported by Rakshit *et al.* [35] where they have obtained the putative minima using the TTM2.1-F force field and optimised the structures further at the MP2/aug-cc-pVTZ level. In Table I we have also compared our values with the lowest energies obtained by various other groups over the years using different levels of theory and we see that our energy values are the lowest of them [36–39].

## III. RESULTS AND DISCUSSION

### A. Structural Properties

The lowest energy structures of  $(\text{H}_2\text{O})_n$  with  $n = 1 - 20$  are presented in Figure 1. The structures for  $n = 2$  to 5 are quasi-planar, linear for  $n = 2$  and cyclic for  $n = 3 - 5$ . From  $n = 6$  we see a significant change in the structural features of these clusters, a transformation into the 3-dimensional structure with respect to the frame of the oxygen atoms is seen. Most of structures can be categorized in to book-shaped, cubic, stacked cubic, stacked pentagonal and cage forms. These structures are preferred over cyclic (or quasi-cyclic) ones as they help maximise the number of H-bonds [45] which reduces the

TABLE I: Comparison of energies (in hartrees) of lowest energy structures of water clusters,  $n = 1 - 20$  obtained in this work, by Rakshit *et al.* [35] and by others [36–39]. (Rounded up to two decimals)

$n$	This work	Rakshit <i>et al.</i> [35]	Others [36–39]
1	-76.45	-76.33	-
2	-152.91	-	-152.73 [39]
3	-229.37	-229.00	-229.11 [39]
4	-305.84	-305.36	-305.49 [39]
5	-382.30	-381.70	-381.86 [39]
6	-458.76	-458.05	-458.24 [39]
7	-535.22	-534.40	-533.68 [37]
8	-611.70	-610.75	-609.93 [37]
			-609.70 [36]
9	-688.16	-687.10	-686.18 [37]
10	-764.63	-763.45	-762.42 [37]
11	-841.09	-839.79	-840.13 [38]
12	-917.56	-916.14	-914.57 [36]
13	-994.02	-992.49	-992.12 [38]
14	-1070.49	-1068.84	-
15	-1146.95	-	-
16	-1223.42	-1221.54	-
17	-1299.88	-1296.73	-
18	-1376.35	-1374.23	-
19	-1452.82	-1450.58	-
20	-1529.28	-1526.93	-

electrostatic repulsion between the negatively charged oxygen, and hence are energetically more favourable. Water molecules are stabilized through a hydrogen bond network [44, 46], which was also observed in our work, indicating the vital role it plays in such clusters. The role of cooperative effects that involve all the nearest neighbours has been observed earlier [47].

There have been various studies on water hexamer, with a varied low energy conformers obtained, depending on the level of theory and the basis set used, e.g. Mhin *et al.* [48] obtained that though low-lying energy hexamers are almost isoenergetic, among them, cyclic hexamer is highly stabilized, while Kim *et al.* [49] have found that the lowest energy structure is cage followed by book ( $\sim$ within 0.1 kcal/mol), however for temperatures above  $\sim 40$  K, book might be more stable than cage. With our chosen level of theory the first 3-dimensional framework of oxygen atoms is seen for the hexamer which has a book-like shape. Interestingly, here the prism-shaped lowest energy structure of hexamer was transformed into a book-shaped form upon geometry optimization [50]. Upon the addition of a water molecule, the new molecule gets attached near its edge leading to the widening of the distance between the edge molecules, forming a pentagon-like shape as shown in Figure 1. However, when one more molecule is added to the heptamer, a significant structural transformation into a nearly cubi-

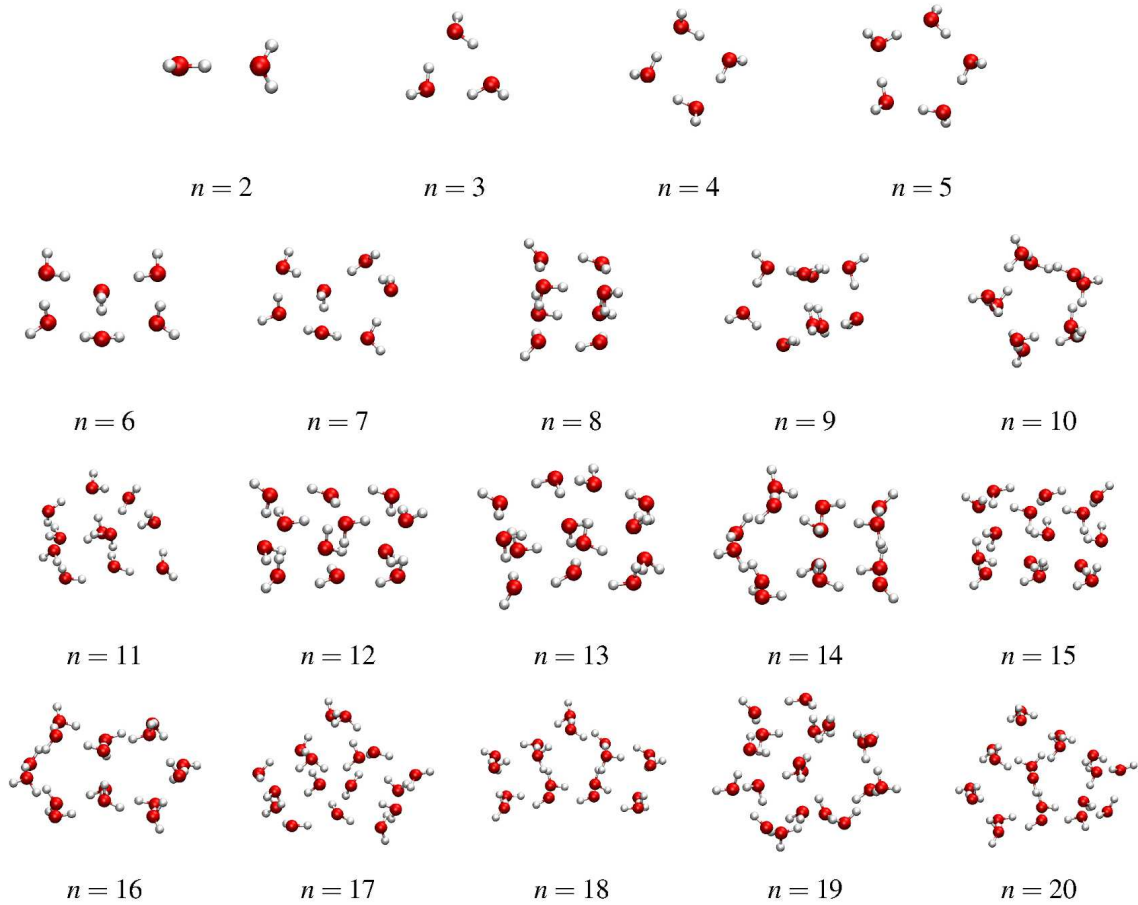


FIG. 1: Optimized geometries of global minimum water clusters  $n = 2 - 20$

cal cage-like structure is seen for the octamer. Further addition of a water molecule distorts the cubical structure. In the decamer cluster, a bilayer pentagonal structure is observed. Thus, as the cluster evolves, symmetrical structures are observed for even-sized clusters such as for  $n = 8$  (nearly cubical),  $n = 10$  (stacked pentagons), and  $n = 12$  (stacked cubical). We also observe that for  $n = 14$ , the structure is composed of squares and pentagons. Interestingly, the odd-sized  $n = 15$  cluster is the only one with a symmetric structure. It forms a 3-stacked-pentagonal structure. A similar structure can be seen in the work by [19, 21]. Table-S1 in the supplementary material provides more information with regards to structure and symmetry, namely point group, bond lengths, bond angle etc. for each cluster.

The stability of the water clusters was examined by analyzing the binding energy per molecule ( $E_b/n$ ), the first and the second derivatives of the total energy as a function of the number of water molecules ( $\Delta E$  and  $\Delta^2 E$ ), hydrogen bond network, the optical gap between the high-

est occupied molecular orbital (HOMO) and the lowest unoccupied molecular orbital (LUMO), VIP, AIP and fragmentation pattern.

To understand the stability of the water clusters, we analyzed the trend in the hydrogen bond network. We plot in Figure 3, the number of oxygen atoms having one and two H-bonds. From these figures, it is clear that up to  $n = 5$ , the O atoms only form 1-H bond whereas for  $n \geq 6$ , the oxygen atoms form 1 or 2 H-bonds, giving the clusters more stability as compared to the ring structures, and which is also responsible for the formation of the hydrogen bond network described by Ludwig *et al.* [46]. Maheshwary *et al.* [44] have performed extensive studies of different isomers, their stabilization energies, and the role played by the H-bonds using different levels of theories such as Hartree-Fock and DFT. They have found that the average number of hydrogen bonds per water molecule increases with size and gets saturated to about 1.8 when  $n \rightarrow 20$ . We also obtain a similar trend as can be seen in Figure 4. The average number of H-bonds per

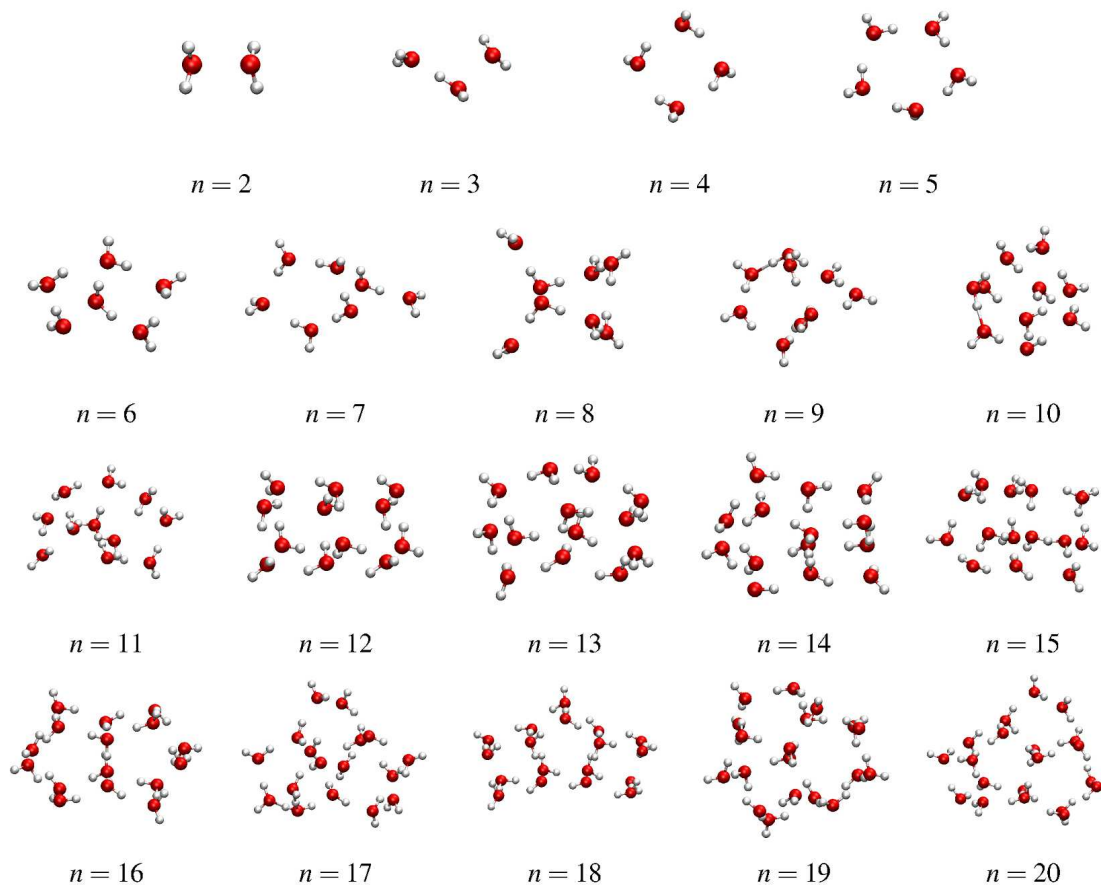


FIG. 2: Optimized geometries of cationic water clusters for  $n = 2 - 20$

O atom increases gradually, and levels off between 1.6 to 1.7. On addition of one molecule to  $n = 19$ , the asymmetric structure becomes nearly symmetric now for  $n = 20$ , on getting even no of molecules, with an average no of H-bonds per O atom increasing from 1.63 for  $n = 19$  to 1.7 for  $n = 20$ , with 14 O-atoms making 2 H-bonds and 6 O-atoms making 1 H-bonds, forming a structure with stacked pentagons and stacked cubic structure.

In addition to this, in order to actually visualize these H-bonds as well as other factors or interactions that contribute to formation of these geometries, we have also performed visual study of non covalent interactions (NCI) using Multiwfn [51] package, and plotted iso-surfaces for strong interactions such as H-bonds between water molecules in clusters, the weak Van der Waals interaction, as well as the strong repulsive forces or the steric effects arising from the closed ring structures. These can be seen in Figure 5. We have shown here small clusters as well as even number of clusters some of which are symmetric. Thus, in dimer we can see an iso-surface of H-bond. Trimer being the smallest ring

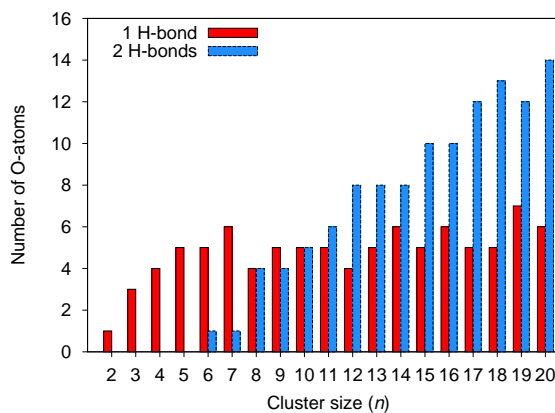


FIG. 3: Number of hydrogen bonds in water clusters with  $n = 2 - 20$

structure and the molecules being close to each other, there is a steric hindrance observed at the center of the cluster, along with the H-bonds between the molecules.

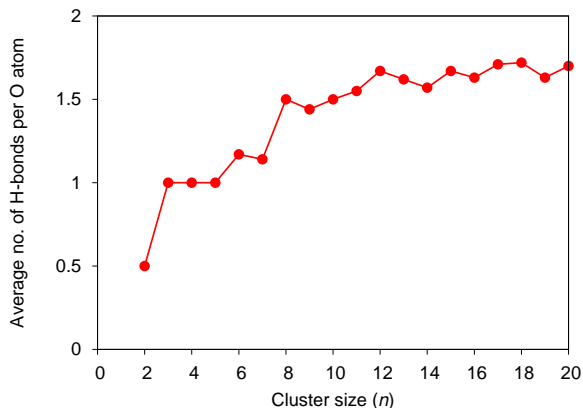


FIG. 4: Average number of hydrogen bonds per oxygen atom in water clusters

As we go further, in tetramer we can also see the weak Van der Waals interaction, at the center, between the H-bonds. The number of iso-surfaces of H-bonds and the Van der Waals interaction go on increasing as we go up to  $n = 20$ . Thus, as we can see from these figures, these non covalent interactions, play an important role in binding the cluster together and giving them stability. The H-bond network leads to the formation of clusters of water molecules and giving it various unique properties at nano-scale.

## B. Energetics

### 1. Binding Energy

To see the stability of water clusters, we have computed the binding energy per molecule in water clusters as a function of cluster size which indicates how easy or difficult it is for the water molecules to form a cluster. It is calculated as follows:  $E_b/n = \frac{1}{n}(E(\text{H}_2\text{O})_n - nE(\text{H}_2\text{O}))$ , where  $E(\text{H}_2\text{O})_n$  is the total interaction energy of the  $n$ -mer water cluster and  $E(\text{H}_2\text{O})$  is the energy of the water monomer. This can be seen in Figure 6.

The experimental value of Binding Energy for dimer has been found at  $-5.4 \pm 0.7$  kcal/mol [33], whereas in the present study we have obtained it to be at  $-5.307$  kcal/mol which is in good agreement. Table-S2 in the supplementary material shows a comparison of binding energies in this work with the results of other researches using various techniques. The energy difference obtained is due to different approximation methods used by each of them. Our method gives binding energies that are

higher than those obtained in reference [15] (except for  $n = 11, 12$  and  $20$ ), employing B3LYP, aug-cc-pVDZ basis set.

It is noted that the increased stability of the clusters as the size increases and approaches the bulk, where it saturates, is in the best agreement with the reported results [52]. However, from Figure 6, we see a greater increase in the  $E_b/n$  for  $n = 4$  because of its square shaped symmetry, and a further notable increase in  $E_b/n$  for  $n = 8$  due to its cubical geometry. As we go further, we see that for even number of clusters, i.e. for  $n = 10, 12, 14, 16, 18$ , the  $E_b/n$  values are slightly greater than their preceding odd numbered motifs.

To support the above arguments and verify the predicted stability of the clusters, we have also calculated binding energies in the form of their first and second energy differences i.e. the energy required to remove one molecule from a cluster and its second order derivative,  $\Delta E$  ( $\Delta E = E_n - (E_{n-1} + E_1)$ ) and  $\Delta^2 E$  ( $\Delta^2 E = E_{n+1} - 2E_n + E_{n-1}$ ) respectively for all water clusters. It is shown in Figure 7. A low value of  $\Delta E$  along with a large value of  $\Delta^2 E$  indicates a stable cluster. Structures and symmetry of the clusters as well as the number of H-bonds that each O atom in the cluster makes, play a major role in determining their binding energies. We see that compared to odd number of clusters, even number of clusters have higher binding energies, except hexamer, with a lower binding energy, due to its book shaped structure which is less stable as an electron can be removed from its edges with less number of co-ordination of H-bonds it makes, i.e. only one O atom makes 2 H-bonds, rest all O-atoms make one H-bonds. Higher binding energy implies higher stability. Octamer, shows higher binding energy with its cubical shape (-ve sign represents the bound state of molecules in the cluster). Similarly tetramer with square shape, dodecamer with stacked pentagons, cluster with  $n = 12$  with stacked cubic,  $n = 14$  with cubic and stacked pentagons,  $n = 16$  with stacked pentagons, and  $n = 19$  with cage structure show high binding energies. Whereas, cluster with  $n = 11$  formed by adding one molecule to the dodecamer can easily be removed and cluster with  $n = 17$  also being an asymmetrical structure, removal of electron does not need much of energy. Thus  $n = 11$  and  $17$  clusters show low binding energy and thus lowest cluster stabilities.

Thus, to summarize, from Figure 6 and 7, we can observe that all the clusters with an even number of water molecules seem to be more stable than the odd-numbered, except for  $n = 2$  and  $6$ . The clusters with  $n = 4, 8, 12, 14, 16$  and  $19$  water molecules are found to be more stable as compared to others. From the literature it can be seen that the cuboid or the fused pentamers or their combination show a greater stability [44]

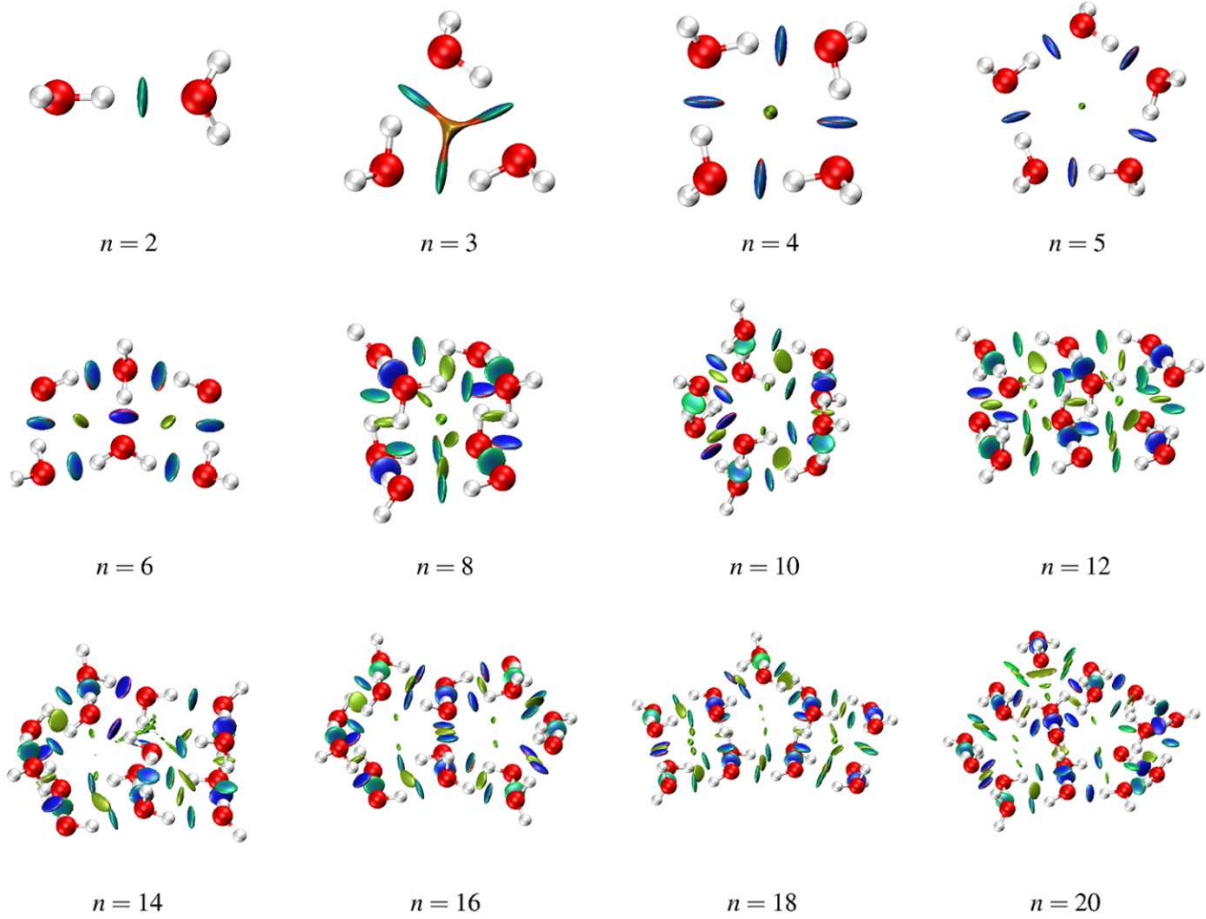


FIG. 5: Here, various colour shades represent different Non Covalent Interactions (NCI). Shades dark blue to dark green represent strong attraction i.e. H-bonds, the light green shades represent weak Van der Waals interaction, the golden to red shades indicate strong repulsive steric effect in ring and cage structures, and the mix of these colours represent an interplay between these interactions.

or the conformers with four membered rings, namely  $n = 4, 8, 12$  are relatively more stable than the other clusters [53]. The central difference approximation has also been used [54] to illustrate that even number of clusters are more stable than the odd numbered, e.g.  $n = 8, 12, 16, 20$ . Thus, we can see that the structure, symmetry of the clusters and the number of H-bonds per O-atom, play a significant role in determining their stability.

## 2. Shape Analysis

We have analyzed the shape of the water clusters using the quadrupole deformation parameter  $\epsilon_d = \frac{2Q_x}{Q_y + Q_z}$ , where  $Q_x \geq Q_y \geq Q_z$  are the eigenvalues of the quadrupole tensor  $Q_{ij} = \sum_I R_{Ii} R_{Ij}$ . Here  $R_{Ii}$  is the  $i^{\text{th}}$  co-

ordinate of ion  $I$  relative to the centre of mass. When all the eigenvalues are equal, i.e.  $Q_x = Q_y = Q_z$ ,  $\epsilon_d = 1$ , Such a system has perfect spherical symmetry. Any deviation of  $\epsilon_d$  from this value indicates quadrupole deformation of some sort. Further insights can be obtained by analyzing the dimensionless Hill-Wheeler parameters [55]. Whether the cluster is oblate or prolate can be determined using the parameters  $\xi = \frac{Q_x - Q_y}{Q_x - Q_z}$ , where  $0 \leq \xi \leq 1$ . The value  $\xi = 0$  corresponds to an oblate structure, whereas  $\xi = 1$  corresponds to a prolate structure. Any value of  $\xi$  between 0 and 1 implies a triaxial deformation. A drawback with this approach is that for spherical structures,  $\xi$  becomes indeterminate and thus can lie anywhere between 0 and 1, and hence it becomes difficult to identify. This can be overcome by analyzing  $\xi$  against another parameter  $q$ , given by  $q^2 = \frac{Q_x^2 + Q_y^2 + Q_z^2}{\text{Tr}(Q)^2}$ . The parameter  $q$  determines the measure of sphericity of

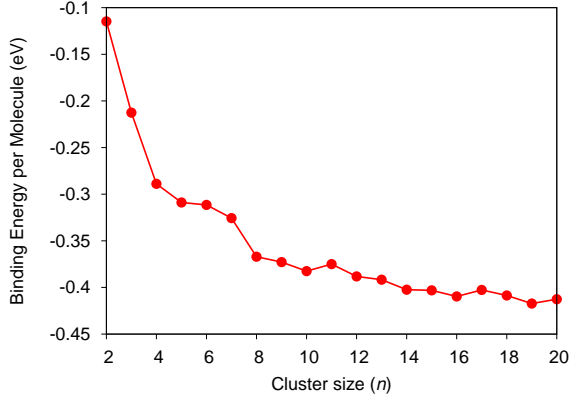


FIG. 6: Binding energy per molecule as a function of cluster size ( $n$ )

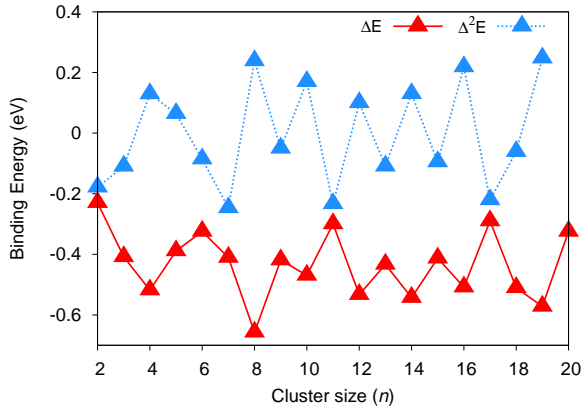


FIG. 7: Binding energy and  $\Delta^2 E$

the system with  $q = 0$ , indicating spherical shape, and as it goes on increasing the structures tend to become less spherical, *i.e.* having a greater deformation. In Figure 8, we have plotted the values of  $\xi$  against  $q$  for all the clusters. One can observe that the structures with  $\xi$  between 1 and 0.5, namely  $n = 13, 14, 15, 16$  and  $18$  have prolate character, whereas those with  $\xi$  between 0 and 0.5, *i.e.*  $n = 10$ , and  $19$  have an oblate character.

Analyzing the contribution of the eigenvalues  $Q_x$ ,  $Q_y$  and  $Q_z$  (refer to Figure-S1 in supplementary material), we can infer that the clusters of sizes  $n = 3, 4$  and  $5$  with  $\xi = 0$  are oblate, whereas  $n = 8$  and  $12$  with  $\xi = 1$  are prolate. For  $n = 8$ , with a  $q$  value of  $0.05$ , indicates a nearly spherical symmetry with a slight distortion of an oblate nature. A similar pattern is also followed by the stacked pentagonal decamer, the nonamer structure, and the cage structure of the  $n = 19$  cluster, albeit with slightly higher distortions. It is interesting to note that most of the clusters whose  $\xi$  and  $q$  values lie in the central region (*i.e.*  $n = 6, 7, 9, 11, 17$  and  $20$  show a sig-

nificant distortion in their structures and are some of the least stable clusters as noted above from figure 7. The 2-dimensional clusters with  $n = 3, 4$  and  $5$  and the first 3-dimensional structure of  $n = 6$  exhibit very high values of the  $q$  parameter indicating a substantial deviation from spherical symmetry. The highest value of  $q = 1.3$  was found for  $n = 18$  which has maximum non-spherical distortions.

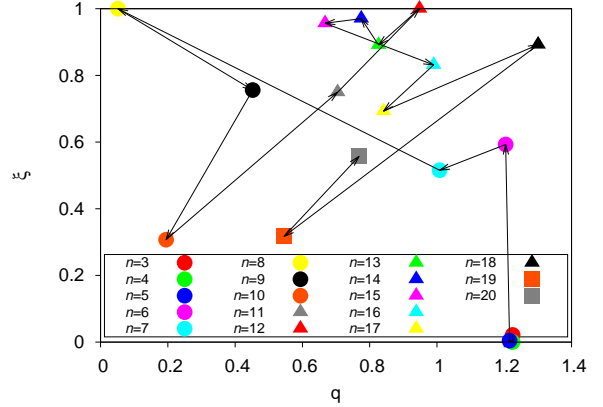


FIG. 8: Shape parameter as a function of deformation of the size of the cluster.

### 3. Fragmentation

Analyzing the fragmentation patterns of water clusters offers valuable insights into their stability. We have calculated the fragmentation energies for all clusters, considering all possible breakups from 2 to  $n$ -fragments, where  $n$  is the number of molecules in the cluster. In figure 9, we present the lowest-energy fragmentation pathways for all clusters, specifically, the breakup into 2, 3, 4 and 5 fragments. The fragmentation energy for  $m$ -fragments is calculated using the following:

$$\Delta E_m^{l_1, l_2, \dots, l_m} = E_n - \sum_{i=1}^m E_{l_i}$$

where,  $\sum_{i=1}^m l_i = n$  with  $m < n$ ,  $l_i$  being the number of molecules in the  $i^{th}$  fragment. The alphabets  $n$  and  $m$  represent cluster size and number of fragments, respectively.  $E_n$  is the total energy of the cluster and  $E_{l_i}$  ( $i = 1 - m$ ) are the energies of the fragments. A large fragmentation energy indicates a strong bonding between the water molecules which in turn makes that cluster more stable. From the figure, we see that for 2 fragments the energy needed to break the clusters is the lowest. As the number of fragments is increased, the fragmentation energy goes on increasing. This is consistent with the experimental results, where the dissociation energies of the neutral wa-



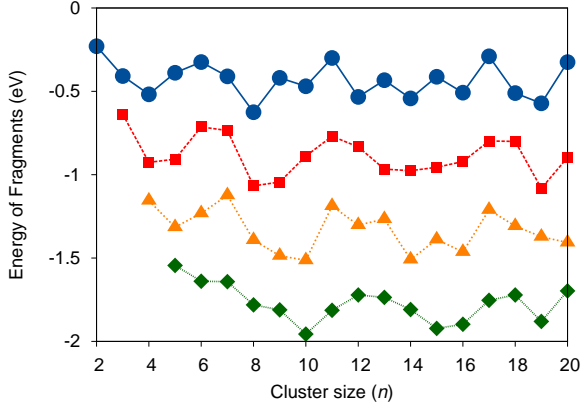


FIG. 9: Fragmentation of water clusters  $n = 2 - 20$  into 2 (Blue), 3 (Red), 4 (Yellow), 5 (Green) fragments respectively

ter clusters in the size range  $n = 2 - 9$  suddenly increase from dimer to trimer, followed by the gradual change in energy with an increase in cluster size [56]. The figure also shows a dip in the fragmentation energies for certain fragment sizes with  $m = 4, 8, 10, 16$  and  $19$ . Incidentally, these clusters were found to be some of the most stable ones (see figure 7).

In figure 10, we show the number of occurrences of all the fragments found in the lowest five channels. The frequency of water monomers is not displayed, as they are the predominant fragment in all channels and represent the most favourable pathway due to their low dissociation energy. The formation of monomers is observed in a multi-step fragmentation process with the loss of a single water molecule by every water cluster. This is followed by the maximum occurrence of the dimer, which is a second-step fragmentation process. As the fragmentation channel increases, the likelihood of large fragment formation decreases, impeded by a substantial potential barrier, when all possible fragmentation pathways are taken into account. However, we also note another interesting feature. Despite the declining trend in the histogram, the occurrence of the fragments  $m = 4, 8, 12$  and  $14$  show higher values than their neighbouring fragments, implying that these fragments are more likely to be observed in fragmentation experiments. These results are consistent with the reported data [17], where the stability of clusters has been explained with the first and second-best fragmentation channels. Thus, a higher fragmentation energy of any fragment indicates the fragment to be more stable. Thus, the fragmentation process shows an increase in the stability with the size of the cluster which supports the observation of binding energy per atom as described above.

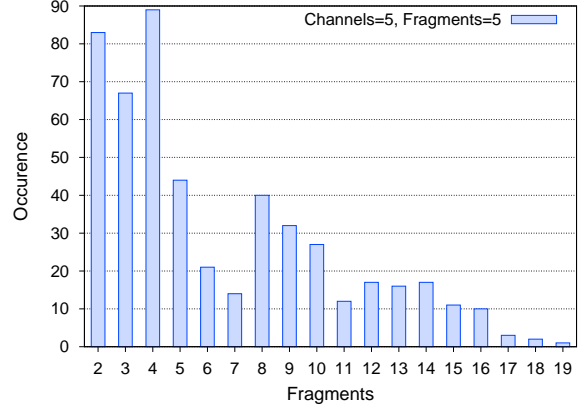


FIG. 10: Frequency of occurrence of different sizes of fragments during fragmentation process for the lowest five channels.

### C. Electronic Properties

The stability of the  $(\text{H}_2\text{O})_n$  clusters is also explained using ionization potential. The energies of neutral and singly charged cationic water clusters were calculated with and without the geometry optimization. Using the energy values from these we calculate the VIP and the AIP respectively. In experiments, it is difficult to measure VIP since such clusters almost undergo instantaneous structural relaxation upon removal of an electron, making the AIP more important for us to study. Figure 11 shows the VIP (red curve) and the AIP (blue curve). Since for the monomer, it gets difficult to remove an electron from its filled molecular orbital, the value of its ionization potential (IP) is the highest, and goes on decreasing with size. It is to be noted that the AIPs are lower than the VIPs. However, for certain sizes such as  $n = 2, 3, 6, 7, 8, 11$  and  $17$ , the difference is much larger. This can be attributed to the significant change in their geometric structures after the removal of an electron (see Figures 1 and 2). For instance, the two molecules in the neutral dimeric cluster are bonded by a single H-bond, whereas in the positively charged form, after structural relaxation, a change in orientation of molecules lead to two H-bonds - one for each O-atom, leading to an increased difference between the VIP and AIP. The neutral trimer cluster forms an equilateral triangle geometry which changes to a scalene triangle upon geometric relaxation after the removal of an electron. On the other hand, the changes in the structure for clusters with sizes  $n = 4$  and  $5$  are insignificant. The experimentally measured [56] appearance energies of neutral water clusters for  $n = 2 - 80$  have been found to converge to around  $10.6 \text{ eV}$  for  $n > 20$ , IP for a single water molecule is  $12.6 \text{ eV}$  [34], whereas the AIP for liquid water has been reported to be at  $9.3 \text{ eV}$  [16]. Incidentally, the ionization

energies, *i.e.* VIP and AIP in our work starts from about 12.95 eV and 12.85 eV for  $n = 1$  and reaches a value of about 9.03 eV and 8.79 eV respectively for  $n = 20$ .

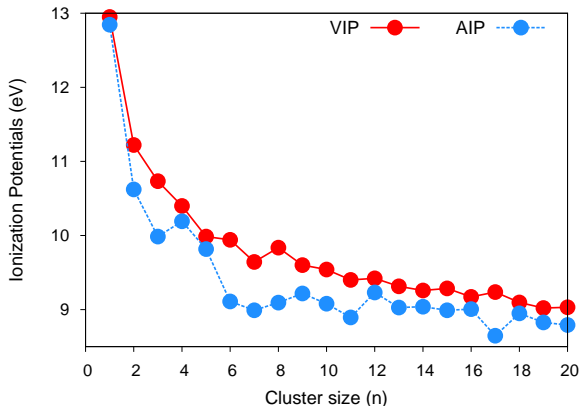


FIG. 11: Vertical and Adiabatic ionization potentials of water clusters for  $n = 1 - 20$

The quantification of eigenvalue spectra allows us to understand the factors that affect the stability of dynamical systems. We have examined the eigenvalue spectrum as a function of cluster size (See Figure-S2 in supplementary material). The red and blue energy levels are identified as the occupied and unoccupied orbitals respectively. From the HOMO-LUMO gap, we can understand the stability of the structure. We see that for dimer it is smaller than that of monomer, indicating that it is less stable. From Figure 12 it can be seen that  $n = 4, 8, 12, 16$  show larger HOMO-LUMO gaps, indicating that they are chemically more stable than the other clusters.

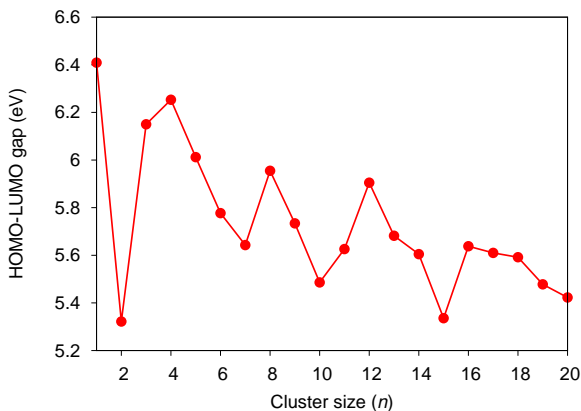


FIG. 12: HOMO-LUMO gap of water clusters

## D. IR Spectra

Vibrational spectroscopy deals with the infrared spectra of the molecules which are specially used for the elucidation of molecular structure. The infrared spectra of the ground state geometries of water clusters with  $n = 1 - 20$  are shown in Figure 13. First, we begin with water monomer followed by clusters with  $n = 2, 4, 8, 12$  and 16 which are found to be the most stable structures from the energetic, fragmentation and HOMO-LUMO gap analysis.

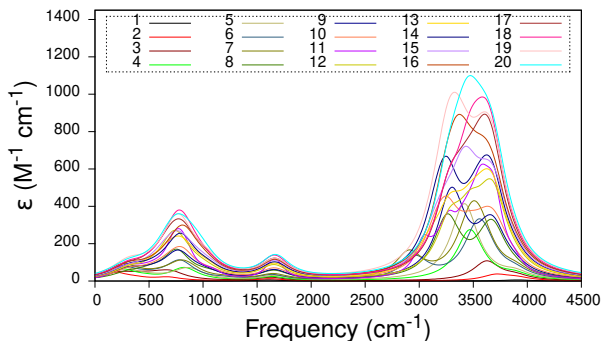


FIG. 13: Infrared spectra of water clusters for  $n = 1 - 20$

In the case of monomer, we observed three IR bands with vibrational modes of bending, symmetric and asymmetric stretching. The frequency of the symmetric and asymmetric stretching modes are  $3813.12 \text{ cm}^{-1}$  and  $3918.87 \text{ cm}^{-1}$  respectively whereas the bending mode is observed to be at  $1602.44 \text{ cm}^{-1}$ . It is also close to the reported experimental and theoretical results [57–59].

In the case of the water dimer, we have observed vibrational and rotational modes. The rotational modes have been observed at a lower frequency range as compared to the vibrational modes. Six rotational modes are lying in the range ( $141\text{--}675 \text{ cm}^{-1}$ ). The four bands at  $3705.57 \text{ cm}^{-1}$  (symmetric),  $3814.40 \text{ cm}^{-1}$  (symmetric),  $3892.69 \text{ cm}^{-1}$  (asymmetric) and  $3915 \text{ cm}^{-1}$  (asymmetric) in the  $(\text{H}_2\text{O})_2$  geometry are ascribed to stretching vibrations and the bands at  $1613.15 \text{ cm}^{-1}$  and  $1629.22 \text{ cm}^{-1}$  are assigned to the bending vibrations of O-H bonds. It is found that our results are in fairly good agreement with those obtained from the theoretical and experimental results [58–61]. It is observed that the bonded H-O-H bending mode of vibration is blue-shifted compared to the water monomer's H-O-H bend. On the other hand, the O-H symmetric and asymmetric stretching modes show red shifts. In the case of water trimer, we have observed H-O-H bending modes at  $1624.24 \text{ cm}^{-1}$ ,  $1629.86 \text{ cm}^{-1}$  and  $1651.96 \text{ cm}^{-1}$ , and six O-H stretching modes between  $3560\text{--}3894 \text{ cm}^{-1}$ . The observed values of the frequencies show blue- and red-shift in the H-O-H

bending and O-H stretching respectively and are consistent with the reported results [61–63].

The H-O-H bending and O-H stretching modes in cyclic water tetramer show a very interesting pattern due to the arrangement of the equivalent hydrogen bonds on the sides of the square. Each O-H group directly couples with its hydrogen bond acceptor partner. The four H-O-H bending and eight O-H stretching modes belong to  $1630\text{--}1681\text{ cm}^{-1}$  and  $3376\text{--}3886\text{ cm}^{-1}$ , respectively, which shows the blue and red-shift for the water monomer, dimer and trimer. All the calculated values of vibrational frequencies are in reasonable agreement with the reported result [57, 63]. Thus, this indicates that increasing the cluster size, which brings in the role of hydrogen bonds, has a substantial effect on the vibrational spectra of water molecules. Two modes of O-H stretching in each case along opposite corners of the square, sides of the square, and inside and outside the plane were observed.

Next, in stable water octamer the IR vibrational spectrum shows that the eight H-O-H bending modes lie in the range  $1634\text{--}1728\text{ cm}^{-1}$ . On the other hand, the sixteen stretching modes belong to  $3204\text{--}3878\text{ cm}^{-1}$ . The calculated values of the vibrational frequency of the stretching modes are in excellent agreement with the reported results [64]. The detailed analysis of the vibrational frequency of the O-H stretching mode is classified into three regions which are associated with free O-H, single donor O-H and double donor O-H groups. It is seen that four free O-H vibrations are nearly degenerate ( $3878.32\text{ cm}^{-1}$ ,  $3878.34\text{ cm}^{-1}$ ,  $3878.41\text{ cm}^{-1}$  and  $3878.73\text{ cm}^{-1}$ ). The four single-donor O-H stretch modes, with their strong, linear H-bonds, have large frequency shifts of  $186\text{ cm}^{-1}$  to  $263\text{ cm}^{-1}$ . On the other hand, the double donor O-H has a higher frequency shift of  $434\text{--}488\text{ cm}^{-1}$  with respect to single donor O-H. It is also observed that there are two nearly degenerate modes in each case (single donor O-H and double donor O-H). It is the highest-frequency single-donor mode, which is nondegenerate ( $3630\text{ cm}^{-1}$  and  $3648\text{ cm}^{-1}$ ). It is also observed that the double-donor vibrations are weaker than the single-donor O-H stretch vibrations because of the weaker, nonlinear H-bonds created when both O-H groups on a given water molecule are involved in H-bonds in a strained structure of water octamer. This results in a gap of  $411\text{ cm}^{-1}$  between single and double donor fundamental frequencies. It is found that the four highest and lowest frequency modes have asymmetric and symmetric O-H stretch character on double donor water molecules. It is observed that the calculated values of the vibrational frequencies of bending and stretching modes are comparable to the reported theoretical values [65].

Now we look at the IR vibrational spectrum of

$(\text{H}_2\text{O})_{12}$ . The vibrational spectrum shows three distinct regions namely, intermolecular vibrations O $\cdots$ H between  $59\text{ cm}^{-1}$  and  $1095\text{ cm}^{-1}$ , a region of intramolecular H-O-H bending modes between  $1639\text{ cm}^{-1}$  and  $1735\text{ cm}^{-1}$ , and a region of intramolecular O-H stretching vibrations between  $3241\text{ cm}^{-1}$  and  $3877\text{ cm}^{-1}$ . All these regions show doubly degenerate modes. The vibrational spectrum of  $(\text{H}_2\text{O})_{16}$  also shows a similar trend, and in addition to it, there is a red-shift of intramolecular bands for the frequency range from  $3241\text{ cm}^{-1}$  to  $3189\text{ cm}^{-1}$ . Previous studies [66, 67] have found that due to the H-bonds formation, the frequency of the H-O-H bending mode increases from gas to liquid phase. As we have seen in our results, we find a similar trend of increase in the H-O-H frequency as the cluster size goes on increasing. It is also stated that, a greater H-O-H bending mode frequency indicates a lower O-H stretching frequency, implying stronger intermolecular H-bonds. In the present work as we have seen blue-shift of H-O-H vibrational mode along with red-shift of O-H stretching mode for  $n = 2, 3, 4, 8, \dots$ , this confirms an increase in the H-bond strength with increasing  $n$ .

## E. Optical Properties

To understand the electronic transitions and its origin, we have carried out TDDFT calculations on the optimized water clusters for  $n = 1 - 20$ , using B3LYP functional [68] and 6311++g(d,p) basis set. The  $n$ -states chosen for each cluster were such that they covered all the states upto the first ionization potential. The origin of optical excitations in these clusters is explained with the help of the eigenvalue spectra, optical bandgap and molecular orbitals (MOs). Table-S3 given in the supplementary material represents the summary of the electronic states of the first three major excitations of water clusters with high oscillator strengths. It shows the VIP and AIP, excitation energy of major transitions ( $E_{\text{exc}}$ ), energy of the most significant peak ( $E_m$ ), oscillator strength ( $f_{\text{osc}}$ ), optical bandgap ( $E_{\text{gopt}}$ ) and excited state compositions, their assignments, along with their percentage contribution. The symbols ‘H’ and ‘L’ stand for the HOMO and the LUMO respectively, and corresponding states below ( $H_1, H_2, \dots$ ) and above ( $L_1, L_2, \dots$ ) these levels. Figure 14 shows the optical spectra of all the clusters.

A number of features can be discerned from the table and the optical spectra. i. The optical bandgap varies from  $7.14\text{ eV}$  to  $8.17\text{ eV}$  which is oscillatory in nature with maximum value at  $n = 4, 8, 12, 16$  and belongs to ultra-violet region. ii. As the cluster size increases for  $n \geq 10$ , the number of spectral lines increases along with line broadening. iii. We find that the optical spectra of

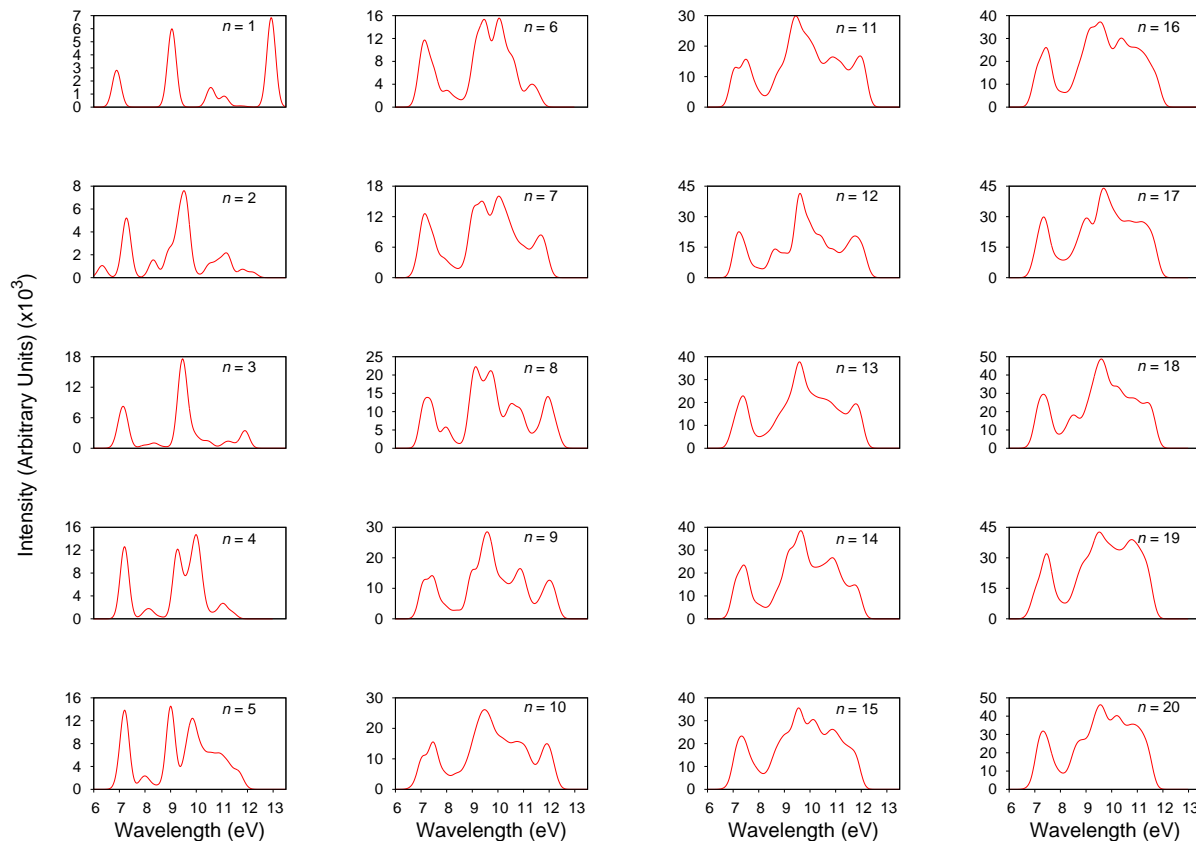


FIG. 14: Optical absorption spectra of water clusters for  $n = 1 - 20$

the stable structures show blue-shifts. This can be attributed to the stability of the clusters. iv. It is also observed that only the stable structures show maximum oscillator strength. v. It is interesting to note that in all the cases the first excitation occurs between HOMO to LUMO. We will now explain and discuss each feature in the next section.

We begin our discussion with water molecule. The absorption spectrum of a fully structurally relaxed monomer can be seen in Figure 14. It shows the three major peaks at 6.89 eV, 9.05 eV and 12.93 eV. The optical bandgap obtained is 8.17 eV, which is within 10% of the experimental value [69]. From Figure 15, it is observed that the first excitation takes place between non-bonding HOMO, which is  $\pi_y$ , to anti-bonding LUMO, that is  $\sigma_z^*$ . The HOMO to LUMO transition is obtained at 6.89 eV (179.88 nm) with oscillator strength of 0.04. The second major transition occurs between  $H_1$  to L, *i.e.*  $\sigma_x$  (bonding) to  $\sigma_z^*$  (anti-bonding) orbital with oscillator strength of 0.09 at 137.01 nm. The third major transition from  $H_2$  (bonding orbital  $\sigma_z$ ) to L (anti-bonding  $\sigma_z^*$ ) involves still higher energy, thus, a further blue-shift is seen, with the highest intensity obtained at

12.93 eV (95.92 nm), with an oscillator strength of 0.10. The other probable electron transitions with their respective oscillator strengths give us different peaks in the UV-VIS spectrum with energy corresponding to the energy difference between those two levels. We can see these energy levels from the eigenvalue spectra.

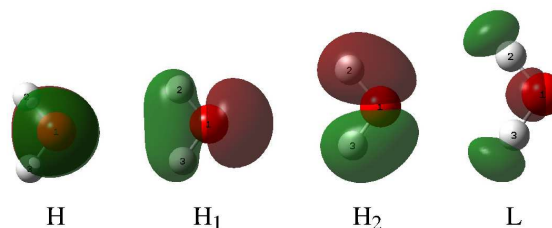


FIG. 15: MOs involved in first three excitations for  $n = 1$ , with percentage contribution  $\geq 50\%$

When two water molecules come together to form a dimer, there is a splitting of energy levels. The HOMO for the dimer is at a higher energy and the LUMO is at a lower energy than that of the monomer. Thus reducing the bandgap as compared to that of monomer and

thus lesser energy is needed for electron transition from HOMO to LUMO, leading to a red shift in the bandgap. In fact, for the dimer, the optical bandgap obtained is the lowest among all the twenty clusters. We can also see an overall red-shift in its optical spectrum. The orbitals involved for the most probable transition, with  $f_{osc} = 0.09$  are mainly contributed by the  $H_3$  and  $L$ , having bonding and anti-bonding character respectively as shown in Figure 16. These orbitals are localized over individual molecules, with  $H_3$  exhibiting  $\sigma_x$  type and  $L$  showing  $\sigma_z^*$  type characteristics. It is the tenth excitation and needs an energy of 9.6 eV (129.2 nm). The second major peak at 7.3 eV is due to excitation from  $H_1 \rightarrow L$ , having  $\sigma_x$  type (bonding) and  $\sigma_z^*$  type (anti-bonding) attributes respectively, with oscillator strength of 0.06. The third major peak with  $f_{osc} = 0.02$  is seen at 11.23 eV due to  $\sigma_x$  type  $H_3$  (bonding orbitals) to  $L_2$  (anti-bonding orbitals) transition.

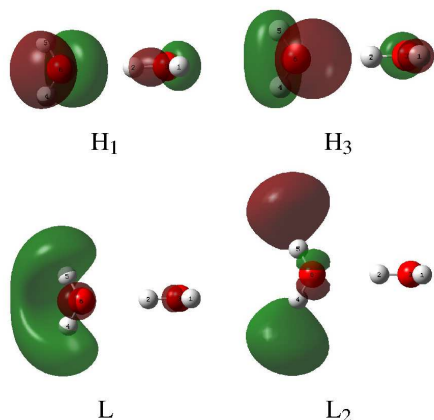


FIG. 16: MOs involved in first three excitations for  $n = 2$ , with percentage contribution  $\geq 50\%$

Going further on to trimer, we find that for  $f_{osc} = 0.12$ , the orbitals involving the electronic transition are  $H_5$  (having bonding) and  $L$  (having anti-bonding character). But it is seen that  $H_4$  and  $H_5$  are nearly degenerate. Because of its equilateral triangle shape or the smallest ring shape, there is an overlap of its  $\sigma_x$  type orbitals over two of its molecules in the  $H_5$  state. This gives it stability, requiring greater energy for electron removal and thus a larger bandgap is observed. Other major contribution for this excitation comes from  $\sigma_x$  type  $H_3$  (bonding orbitals) and  $L_1$  (anti-bonding orbitals).

For tetramer, the HOMO belongs to a set of four degenerate orbitals-  $H$  to  $H_3$  (all having non-bonding attributes), which again is the reason for greater stability of the cluster, thus needing higher energy for excitation. This can also be seen from the percentage contribution of MOs involved in the highest probable transition having  $f_{osc} = 0.1$  at 9.98 eV, with major contributions com-

ing from  $H \rightarrow L_5$ ,  $H_1 \rightarrow L_6$ ,  $H_2 \rightarrow L_7$  with 34.56%, 26.49%, 23.54% respectively. The second major peak is due to the excitation of bonding  $H_6$  to anti-bonding  $L$  with  $f_{osc} = 0.09$ . The third highest peak comes from the transition  $H_1 \rightarrow L$  (non-bonding to anti-bonding orbitals respectively) with oscillator strength of 0.07. Here,  $H$ ,  $H_1$ ,  $H_2$  have  $\pi_y$  type properties,  $H_6$  has  $\sigma_x$  like character, while  $L$  has  $\sigma_z^*$  like attributes. MOs with contribution of 50% or more in the electronic excitation are given in Figure 17.

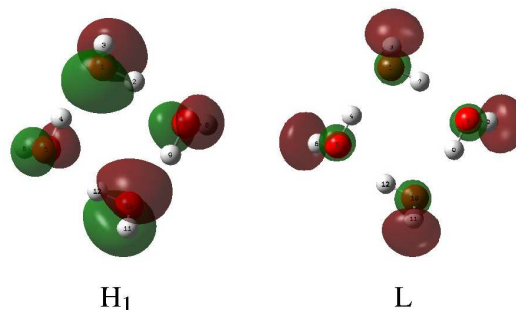


FIG. 17: MOs involved in first three excitations for  $n = 4$ , with percentage contribution  $\geq 50\%$

Going on to our next most stable cluster- octamer, owing to its cubical shape as well as the degenerate energy levels, excitation of electrons from bonding  $H_{14}$  ( $\sigma_x$  type) to anti-bonding  $L$  (with  $\sigma_z^*$  like qualities, refer to Figure 18) gives a notable large value of oscillator strength = 0.18, which turns out to be the second highest value among all the twenty clusters. Similarly the other major peaks are from the other degenerate orbitals, namely bonding ( $\sigma_x$  type)  $H_{11}$  to  $L$  and non-bonding ( $\pi_y$  type)  $H_7$  to  $L$  with  $f_{osc} = 0.10$  and 0.09 respectively.

For  $n = 12$ , the highest oscillator strength value among all the twenty clusters is obtained here, with a value of 0.26 due to the bonding  $H_{19}$  with  $\sigma_x$  like character, which belongs to the set of degenerate orbitals and which corresponds to the excitation of  $H_{19} \rightarrow L$ . The other major peaks are again obtained by the orbitals belonging to degenerate energy levels, namely  $H_1$  and  $H_8$  (both  $\pi_y$  type) showing excitation to the LUMO state (having  $\sigma_z^*$  like attributes).

When we see the optical bandgap diagram (Figure-S3 in the supplementary material), as the number of clusters goes on increasing, except for  $n = 3, 4, 8, 12, 16, 18$  where there are blue-shifts observed due to the reasons explained above, there is a declining trend of the bandgap. It slowly decreases as the cluster size increases and reaches 7.4 eV for  $(H_2O)_{20}$ . This decrease in the energies can be explained by the number of eigenstates that get added as  $n$  increases, forming a band-like structure

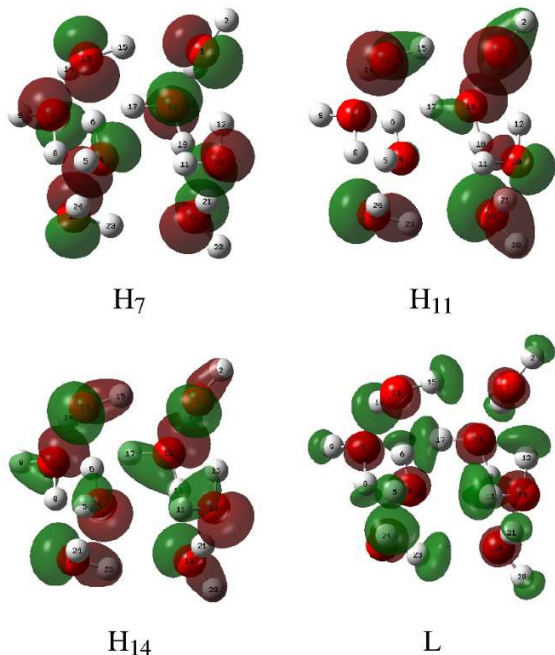


FIG. 18: MOs involved in first three excitations for  $n = 8$ , with percentage contribution  $\geq 50\%$

as it approaches the bulk system, which leads to HOMO-LUMO coming closer to each other, and thus a red-shift in the eigenvalues observed. This is also the reason that in the optical spectra, in Figure 14, for  $n > 10$ , the excitations with higher energies show red-shift. This is comparable from the theoretical bandgap of 7.3 eV for liquid water, and with the experimentally obtained value of 6.9 eV [31]. A similar declining trend in the HOMO-LUMO gap has been observed in a theoretical work by Cabral do Couto *et al.* [70] where they have extrapolated it for  $n = 30$ .

#### IV. SUMMARY AND CONCLUSION

We generated several thousand structures for each of the water clusters within a size range of  $N = 2 - 20$ , using the artificial bee colony algorithm with the classical TIP4P force field. The first 10 lowest-energy structures were further optimized using an *ab initio* method implemented in the Gaussian code with the HCTH exchange-correlation functional and the 6-311++G(d,p) basis set

to obtain the lowest equilibrium geometry. Our results show that the equilibrium geometries obtained during the structural search are lowest in energy than the previously reported results. We reported the structural, electronic, vibrational and optical properties of these lowest equilibrium geometries. The structural stability of cluster was studied using various descriptors such as binding energy, ionization potentials, fragmentation energy, first and second energy difference, vibrational and optical spectra. We also calculated the shape deformation parameter to find the shape of these clusters.

The binding energy per molecule shows the sharp rise up to  $N=10$ . For  $N>10$ , there is a slight increase in it. The energetic analysis shows that clusters with  $N = 4, 8, 12, 14, 16$  and  $19$  are more stable. The analysis of fragmentation energies of the clusters also support these findings. The detailed analysis of the non covalent interactions (hydrogen bonds) finds that it plays a very crucial role in stabilizing the water clusters. We also confirmed the stability of these clusters using frequency analysis from vibrational spectroscopy studies. Infrared spectroscopy reveals three distinct bands in water clusters: intermolecular O...H vibrations ( $23-1191 \text{ cm}^{-1}$ ), intramolecular H-O-H bending ( $1600-1741 \text{ cm}^{-1}$ ) and O-H stretching ( $3229-3877 \text{ cm}^{-1}$ ). The spectra show the strongest intensity for the lowest frequency symmetric stretching modes, along with a red-shift in the stretching vibrations.

We calculated the absorption spectra of these clusters using the B3LYP exchange-correlation functional. The optical bandgap ranges from 7.14 eV to 8.17 eV, belongs to the ultraviolet region. As expected, line broadening occurs for clusters with  $n \geq 10$ , showing an increase in spectral lines. Notably, only the stable clusters exhibit maximum oscillator strength. In all cases, the first excitation corresponds to a  $\pi \rightarrow \sigma^*$  transition.

#### ACKNOWLEDGMENTS

One of the authors VKB acknowledges University of Mumbai for providing UGC fellowship and DST for Junior Research Fellowship (JRF) under DST-PURSE research program for partial funding of this work. We are pleased to acknowledge the National Param Supercomputing Facility (NPSF), CDAC, Pune, India, for providing computing facility. Some parts of the present work have been carried out using NPSF, CDAC, Pune.

[1] Emiliano Brini, Christopher J Fennell, Marivi Fernandez-Serra, Barbara Hribar-Lee, Miha Luksic, and Ken A Dill.

- ture and energies. *Chem. Rev.*, 117(19):12385–12414, 2017. doi:10.1021/acs.chemrev.7b00259.
- [2] Michael D Fayer and Nancy E Levinger. Analysis of water in confined geometries and at interfaces. *Annu. Rev. Anal. Chem.*, 3(1):89–107, 2010. doi:10.1146/annurev-anchem-070109-103410.
- [3] Min Wei, Fan Jin, Tingwei Chen, and Yuchen Ma. Variation of optical spectra of water clusters with size from many-body Green’s function theory. *J. Chem. Phys.*, 148(22):224302, 2018. doi:10.1063/1.5031083.
- [4] Kenneth D Jordan. Smallest water clusters supporting the ice I structure. *Proc. Natl. Acad. Sci.*, 116(49):24383–24385, 2019. doi:10.1073/pnas.1918178116.
- [5] Daniel R Moberg, Daniel Becker, Christoph W Dierking, Florian Zurheide, Bernhard Bandow, Udo Buck, Arpa Hudait, Valeria Molinero, Francesco Paesani, and Thomas Zeuch. The end of ice I. *Proc. Natl. Acad. Sci.*, 116(49):24413–24419, 2019. doi:10.1073/pnas.1914254116.
- [6] Martin F Chaplin. Water: its importance to life. *Biochem. Mol. Biol. Educ.*, 29(2):54–59, 2001. doi:10.1016/S1470-8175(01)00017-0.
- [7] Yaakov Levy and José N Onuchic. Water and proteins: A love–hate relationship. *Proc. Natl. Acad. Sci.*, 101(10):3325–3326, 2004. doi:10.1073/pnas.0400157101.
- [8] Y Pocker. Water in enzyme reactions: biophysical aspects of hydration-dehydration processes. *Cell. Mol. Life Sci.*, 57:1008–1017, 2000. doi:10.1007/PL00000741.
- [9] Nathan I Hammer, Joong-Won Shin, Jeffrey M Headrick, Eric G Diken, Joseph R Roscioli, Gary H Weddle, and Mark A Johnson. How do small water clusters bind an excess electron? *Science*, 306(5696):675–679, 2004. doi:10.1126/science.1102792.
- [10] Victoria Buch, Bauerecker Sigurd, J Paul Devlin, Udo Buck, and Jan K Kazimirski. Solid water clusters in the size range of tens–thousands of  $\text{H}_2\text{O}$ : a combined computational/spectroscopic outlook. *Int. Rev. Phys. Chem.*, 23(3):375–433, 2004. doi:10.1080/01442350412331316124.
- [11] Veronica Vaida. Perspective: Water cluster mediated atmospheric chemistry. *J. Chem. Phys.*, 135(2):020901, 07 2011. doi:10.1063/1.3608919.
- [12] Pablo G Debenedetti and H Eugene Stanley. Supercooled and glassy water. *Phys. Today*, 56(6):40–46, 2003. doi:10.1063/1.1595053.
- [13] Gabriel O. Gomes, H Eugene Stanley, and Mariano de Souza. Enhanced Grüneisen parameter in supercooled water. *Sci. Rep.*, 9(1):12006, 2019. doi:10.1038/s41598-019-48353-4.
- [14] Laurent Canale, J Comtet, A Niguès, C Cohen, Christophe Clanet, A Siria, and L Bocquet. Nanorheology of interfacial water during ice gliding. *Phys. Rev. X*, 9(4):041025, 2019. doi:10.1103/PhysRevX.9.041025.
- [15] Annika Lenz and Lars Ojamae. A theoretical study of water clusters: the relation between hydrogen-bond topology and interaction energy from quantum-chemical computations for clusters with up to 22 molecules. *Phys. Chem. Chem. Phys.*, 7(9):1905–1911, 2005. doi:10.1039/B502109J.
- [16] Javier Segarra-Martí, Manuela Merchan, and Daniel Roca-Sanjuan. Ab initio determination of the ionization potentials of water clusters  $(\text{H}_2\text{O})_n$  ( $n=2-6$ ). *J. Chem. Phys.*, 136(24):244306, 2012. doi:10.1063/1.4730301.
- [17] Xiaojie Liu, Wen-Cai Lu, CZ Wang, and KM Ho. Energetic and fragmentation stability of water clusters  $(\text{H}_2\text{O})_n$ ,  $n=2-30$ . *Chem. Phys. Lett.*, 508(4-6):270–275, 2011. doi:10.1016/j.cplett.2011.04.055.
- [18] Cristiane Ferreira, Hugo FMC Martiniano, Benedito J Costa Cabral, and Vincenzo Aquilanti. Electronic excitation and ionization of hydrogen peroxide–water clusters: Comparison with water clusters. *Int. J. Quantum Chem.*, 111(7-8):1824–1835, 2011. doi:10.1002/qua.22844.
- [19] David J Wales and Matthew P Hodges. Global minima of water clusters  $(\text{H}_2\text{O})_n$ ,  $n \leq 21$ , described by an empirical potential. *Chem. Phys. Lett.*, 286(1-2):65–72, 1998. doi:10.1016/S0009-2614(98)00065-7.
- [20] Tim James, David J Wales, and Javier Hernández-Rojas. Global minima for water clusters  $(\text{H}_2\text{O})_n$ ,  $n \leq 21$ , described by a five-site empirical potential. *Chem. Phys. Lett.*, 415(4-6):302–307, 2005. doi:10.1016/j.cplett.2005.09.019.
- [21] H Kabrede and R Hentschke. Global minima of water clusters  $(\text{H}_2\text{O})_n$ ,  $n \leq 25$ , described by three empirical potentials. *J. Phys. Chem. B*, 107(16):3914–3920, 2003. doi:10.1021/jp027783q.
- [22] Julius T Su, Xin Xu, and William A Goddard. Accurate energies and structures for large water clusters using the X3LYP hybrid density functional. *J. Phys. Chem. A*, 108(47):10518–10526, 2004. doi:10.1021/jp047502+.
- [23] Freddy F Guimarães, Jadson C Belchior, Roy L Johnston, and Christopher Roberts. Global optimization analysis of water clusters  $(\text{H}_2\text{O})_n$  ( $11 \leq n \leq 13$ ) through a genetic evolutionary approach. *J. Chem. Phys.*, 116(19):8327–8333, 2002. doi:10.1063/1.1471240.
- [24] Arshad Khan. Examining the cubic, fused cubic, and cage structures of  $(\text{H}_2\text{O})_n$  for  $n=8, 9, 12, 16, 20$ , and 21: Do fused cubic structures form? *J. Phys. Chem.*, 99(33):12450–12455, 1995. doi:10.1021/j100033a013.
- [25] Albert Defusco, Daniel P Schofield, and Kenneth D Jordan. Comparison of models with distributed polarizable sites for describing water clusters. *Mol. Phys.*, 105(19-22):2681–2696, 2007. doi:10.1080/00268970701620669.
- [26] Note1. The HCTH functional refers to HCTH/407. See reference [27–30].
- [27] Fred A Hamprecht, Aron J Cohen, David J Tozer, and Nicholas C Handy. Development and assessment of new exchange–correlation functionals. *J. Chem. Phys.*, 109(15):6264–6271, 1998. doi:10.1063/1.477267.
- [28] A Daniel Boese, Nikos L Doltsinis, Nicholas C Handy, and Michiel Sprik. New generalized gradient approximation functionals. *J. Chem. Phys.*, 112(4):1670–1678, 2000. doi:10.1063/1.480732.
- [29] A Daniel Boese and Nicholas C Handy. A new parametrization of exchange–correlation generalized gradient approximation functionals. *J. Chem. Phys.*, 114(13):5497–5503, 2001. doi:10.1063/1.1347371.
- [30] A Daniel Boese and Nicholas C Handy. New exchange–correlation density functionals: The role of the kinetic-energy density. *J. Chem. Phys.*, 116(22):9559–9569, 2002. doi:10.1063/1.1476309.
- [31] Changming Fang, Wun-Fan Li, Rik S Koster, Jiří Klimeš, Alfons Van Blaaderen, and Marijn A Van Huis. The

- accurate calculation of the band gap of liquid water by means of GW corrections applied to plane-wave density functional theory molecular dynamics simulations. *Phys. Chem. Chem. Phys.*, 17(1):365–375, 2015. doi:10.1039/C4CP04202F.
- [32] Mohan Chen, Hsin-Yu Ko, Richard C Remsing, Marcos F Calegari Andrade, Biswajit Santra, Zhaoru Sun, Annabella Selloni, Roberto Car, Michael L Klein, John P Perdew, et al. Ab initio theory and modeling of water. *Proc. Natl. Acad. Sci.*, 114(41):10846–10851, 2017. doi:10.1073/pnas.1712499114.
- [33] LA Curtiss, DJ Frurip, and M Blander. Studies of molecular association in H<sub>2</sub>O and D<sub>2</sub>O vapors by measurement of thermal conductivity. *J. Chem. Phys.*, 71(6):2703–2711, 1979. doi:10.1063/1.438628.
- [34] Hisashi Hayashi, Noboru Watanabe, Yasuo Udagawa, and C-C Kao. The complete optical spectrum of liquid water measured by inelastic X-ray scattering. *Proc. Natl. Acad. Sci.*, 97(12):6264–6266, 2000. doi:10.1073/pnas.110572097.
- [35] Avijit Rakshit, Pradipta Bandyopadhyay, Joseph P Heindel, and Sotiris S Xantheas. Atlas of putative minima and low-lying energy networks of water clusters  $n=3-25$ . *J. Chem. Phys.*, 151(21):214307, 2019. doi:10.1063/1.5128378.
- [36] CJ Tsai and KD Jordan. Theoretical study of small water clusters: low-energy fused cubic structures for (H<sub>2</sub>O)<sub>n</sub>,  $n=8, 12, 16$ , and  $20$ . *J. Phys. Chem.*, 97(20):5208–5210, 1993. doi:10.1021/j100122a005.
- [37] Joanna Sadlej, Victoria Buch, JK Kazimirski, and Udo Buck. Theoretical study of structure and spectra of cage clusters (H<sub>2</sub>O)<sub>n</sub>,  $n=7-10$ . *J. Phys. Chem. A*, 103(25):4933–4947, 1999. doi:10.1021/jp990546b.
- [38] Satya Bulusu, Soohaeng Yoo, Edo Aprà, Sotiris Xantheas, and Xiao Cheng Zeng. Lowest-energy structures of water clusters (H<sub>2</sub>O)<sub>11</sub> and (H<sub>2</sub>O)<sub>13</sub>. *J. Phys. Chem. A*, 110(42):11781–11784, 2006. doi:10.1021/jp0655726.
- [39] Sotiris S Xantheas, Christian J Burnham, and Robert J Harrison. Development of transferable interaction models for water. II. Accurate energetics of the first few water clusters from first principles. *J. Chem. Phys.*, 116(4):1493–1499, 2002. doi:10.1063/1.1423941.
- [40] Jun Zhang and Michael Dolg. ABCluster: the artificial bee colony algorithm for cluster global optimization. *Phys. Chem. Chem. Phys.*, 17(37):24173–24181, 2015. doi:10.1039/C5CP04060D.
- [41] William L Jorgensen, Jayaraman Chandrasekhar, Jeffrey D Madura, Roger W Impey, and Michael L Klein. Comparison of simple potential functions for simulating liquid water. *J. Chem. Phys.*, 79:926, 1983. doi:doi.org/10.1063/1.445869.
- [42] M. J. Frisch, G. W. Trucks, H. B. Schlegel, G. E. Scuseria, M. A. Robb, J. R. Cheeseman, J. A. Montgomery, Jr., T. Vreven, K. N. Kudin, J. C. Burant, J. M. Millam, S. S. Iyengar, J. Tomasi, V. Barone, B. Mennucci, M. Cossi, G. Scalmani, N. Rega, G. A. Petersson, H. Nakatsuji, M. Hada, M. Ehara, K. Toyota, R. Fukuda, J. Hasegawa, M. Ishida, T. Nakajima, Y. Honda, O. Kitao, H. Nakai, M. Klene, X. Li, J. E. Knox, H. P. Hratchian, J. B. Cross, V. Bakken, C. Adamo, J. Jaramillo, R. Gomperts, R. E. Stratmann, O. Yazyev, A. J. Austin, R. Cammi, C. Pomelli, J. W. Ochterski, P. Y. Ayala, K. Morokuma, G. A. Voth, P. Salvador, J. J. Dannenberg, V. G. Zakrzewski, S. Dapprich, A. D. Daniels, M. C. Strain, O. Farkas, D. K. Malick, A. D. Rabuck, K. Raghavachari, J. B. Foresman, J. V. Ortiz, Q. Cui, A. G. Baboul, S. Clifford, J. Cioslowski, B. B. Stefanov, G. Liu, A. Liashenko, P. Piskorz, I. Komaromi, R. L. Martin, D. J. Fox, T. Keith, M. A. Al-Laham, C. Y. Peng, A. Nanayakkara, M. Challacombe, P. M. W. Gill, B. Johnson, W. Chen, M. W. Wong, C. Gonzalez, and J. A. Pople. Gaussian 03, Revision c.02. Gaussian, Inc., Wallingford, CT, 2004.
- [43] Karen L Schuchardt, Brett T Didier, Todd Elsethagen, Lisong Sun, Vidhya Gurumoorthi, Jared Chase, Jun Li, and Theresa L Windus. Basis set exchange: a community database for computational sciences. *J. Chem. Inf. Model.*, 47(3):1045–1052, 2007. doi:10.1021/ci600510j.
- [44] Shruti Maheshwary, Nitin Patel, Narayanasami Sathya-murthy, Anant D Kulkarni, and Shridhar R Gadre. Structure and stability of water clusters (H<sub>2</sub>O)<sub>n</sub>,  $n=8-20$ : An ab initio investigation. *J. Phys. Chem. A*, 105(46):10525–10537, 2001. doi:10.1021/jp013141b.
- [45] Garrett D Santis, Kristina M Herman, Joseph P Heindel, and Sotiris S Xantheas. Descriptors of water aggregation. *J. Chem. Phys.*, 160(5):054306, 2024. doi:10.1063/5.0179815.
- [46] Ralf Ludwig. Water: From clusters to bulk. *Angew. Chem., Int. Ed.*, 40(10):1808–1827, 2001. doi:10.1002/1521-3773(20010518)40:10<1808::AID-ANIE1808>3.0.CO;2-1.
- [47] Vasilii S Znamenskiy and Michael E Green. Quantum calculations on hydrogen bonds in certain water clusters show cooperative effects. *J. Chem. Theory Comput.*, 3(1):103–114, 2007. doi:10.1021/ct600139d.
- [48] Byung Jin Mhin, Jongseob Kim, Sik Lee, Jin Yong Lee, and Kwang S Kim. What is the global minimum energy structure of the water hexamer? The importance of non-additive interactions. *J. Chem. Phys.*, 100(6):4484–4486, 1994. doi:10.1063/1.466279.
- [49] Jongseob Kim and Kwang S Kim. Structures, binding energies, and spectra of isoenergetic water hexamer clusters: Extensive ab initio studies. *J. Chem. Phys.*, 109(14):5886–5895, 1998. doi:10.1063/1.477211.
- [50] Jerzy Leszczynski, Anna Kaczmarek-Kedziera, Tomasz Puzyn, Manthos G. Papadopoulos, Heribert Reis, and Manoj K. Shukla, editors. *Handbook of computational chemistry*. Springer Cham, Switzerland, 2017. doi:https://doi.org/10.1007/978-3-319-27282-5.
- [51] Tian Lu and Feiwu Chen. Multiwfn: A multifunctional wavefunction analyzer. *J. Comput. Chem.*, 33(5):580–592, 2012. doi:10.1002/jcc.22885.
- [52] WA Adeagbo and P Entel. Determination of melting of water clusters using density functional theory. *Phase Transitions*, 77(1-2):63–79, 2004. doi:10.1080/01411590310001622473a.
- [53] Chengteh Lee, Han Chen, and George Fitzgerald. Chemical bonding in water clusters. *J. Chem. Phys.*, 102(3):1266–1269, 1995. doi:10.1063/1.468914.
- [54] Sergey Kazachenko and Ajit J Thakkar. Improved minima-hopping. TIP4P water clusters, (H<sub>2</sub>O)<sub>n</sub> with  $n \leq 37$ . *Chem. Phys. Lett.*, 476(1-3):120–124, 2009. doi:10.1016/j.cplett.2009.06.026.



- [55] Aage Niels Bohr and Ben R Mottelson. *Nuclear Structure (in 2 volumes)*. World Scientific Publishing Company, Singapore, 1998. doi:10.1142/3530.
- [56] Leonid Belau, Kevin R Wilson, Stephen R Leone, and Musahid Ahmed. Vacuum ultraviolet (VUV) photoionization of small water clusters. *J. Phys. Chem. A*, 111(40):10075–10083, 2007. doi:10.1021/jp075263v.
- [57] Katharina E Otto, Zhifeng Xue, Philipp Zielke, and Martin A Suhm. The Raman spectrum of isolated water clusters. *Phys. Chem. Chem. Phys.*, 16:9849, 2014. doi:10.1039/C3CP54272F.
- [58] K. Kim and K. D. Jordan. Comparison of density functional and MP2 calculations on the water monomer and dimer. *J. Phys. Chem.*, 98:10089, 1994. doi:10.1021/j100091a024.
- [59] J Paul Devlin, Joanna Sadlej, and Victoria Buch. Infrared spectra of large H<sub>2</sub>O clusters: new understanding of the elusive bending mode of ice. *J. Phys. Chem. A*, 105(6):974–983, 2001. doi:10.1021/jp003455j.
- [60] WS Benedict, N Gailar, and Earle K Plyler. Rotation-vibration spectra of deuterated water vapor. *J. Chem. Phys.*, 24(6):1139–1165, 1956. doi:10.1063/1.1742731.
- [61] J. Coleman Howard, Jordan D. Enyard, and Gregory S. Tschumper. Assessing the accuracy of some popular DFT methods for computing harmonic vibrational frequencies of water clusters. *J. Chem. Phys.*, 143(21):214103, 2015. doi:10.1063/1.4936654.
- [62] Anamika Mukhopadhyay, Sotiris S. Xantheas, and Richard J. Saykally. The water dimer II: Theoretical investigations. *Chem. Phys. Lett.*, 700:163, 2018. doi:10.1016/j.cplett.2018.03.057.
- [63] J. Coleman Howard and Gregory S. Tschumper. Benchmark Structures and Harmonic Vibrational Frequencies Near the CCSD(T) Complete Basis Set Limit for Small Water Clusters: (H<sub>2</sub>O)<sub>n</sub> = 2, 3, 4, 5, 6. *J. Chem. Theory Comput.*, 11(5):2126–2136, 2015. doi:10.1021/acs.jctc.5b00225.
- [64] Christopher J Gruenloh, Joel R Carney, Fredrick C Hagemeister, Caleb A Arrington, Timothy S Zwier, Sharon Y Fredericks, John T Wood III, and Kenneth D Jordan. Resonant ion-dip infrared spectroscopy of the S<sub>4</sub> and D<sub>2</sub>d water octamers in benzene-(water)<sub>8</sub> and benzene<sub>2</sub>-(water)<sub>8</sub>. *J. Chem. Phys.*, 109(16):6601–6614, 1998. doi:10.1063/1.477346.
- [65] Hubert Cybulski and Joanna Sadlej. On the calculations of the vibrational Raman spectra of small water clusters. *Chem. Phys.*, 342:163, 2007. doi:10.1016/j.chemphys.2007.09.058.
- [66] Takakazu Seki, Kuo-Yang Chiang, Chun-Chieh Yu, Xiaoping Yu, Masanari Okuno, Johannes Hunger, Yuki Nagata, and Mischa Bonn. The bending mode of water: A powerful probe for hydrogen bond structure of aqueous systems. *J. Phys. Chem. Lett.*, 11(19):8459–8469, 2020. doi:10.1021/acs.jpcclett.0c01259.
- [67] Michael Falk. The frequency of the H O H bending fundamental in solids and liquids. *Spectrochim. Acta, Part A*, 40(1):43–48, 1984. doi:10.1016/0584-8539(84)80027-6.
- [68] Rüdiger Bauernschmitt and Reinhart Ahlrichs. Treatment of electronic excitations within the adiabatic approximation of time dependent density functional theory. *Chem. Phys. Lett.*, 256(4-5):454–464, 1996. doi:10.1016/0009-2614(96)00440-X.
- [69] A Hermann, WG Schmidt, and P Schwerdtfeger. Resolving the optical spectrum of water: Coordination and electrostatic effects. *Phys. Rev. Lett.*, 100(20):207403, 2008. doi:10.1103/PhysRevLett.100.207403.
- [70] P Cabral do Couto, SG Estácio, and BJ Costa Cabral. The Kohn-Sham density of states and band gap of water: From small clusters to liquid water. *J. Chem. Phys.*, 123(5):054510, 2005. doi:10.1063/1.1979487.